Special Collection

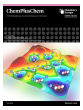

Photochemistry of a 9-Dithianyl-Pyronin Derivative: A Cornucopia of Reaction Intermediates Lead to Common Photoproducts

Marek Martínek,[a, b] Jiří Váňa,[c] Peter Šebej,[b] Rafael Navrátil,[d] Tomáš Slanina,[a, b] Lucie Ludvíková,[a, b] Jana Roithová,*[e] and Petr Klán*[a, b]

Leaving groups attached to the *meso*-methyl position of many common dyes, such as xanthene, BODIPY, or pyronin derivatives, can be liberated upon irradiation with visible light. However, the course of phototransformations of such photoactivatable systems can be quite complex and the identification of reaction intermediates or even products is often neglected. This paper exemplifies the photochemistry of a 9-dithianyl-pyronin derivative, which undergoes an oxidative transformation at the *meso*-position to give a 3,6-diamino-9*H*-xanthen-9-one derivative, formic acid, and carbon monoxide as the main photoproducts. The course of this multi-photon multi-step reaction was studied under various conditions by steady-state and time-resolved optical spectroscopy, mass spectrometry and NMR spectroscopy to understand the effects of solvents and molecular oxygen on individual steps. Our analyses have revealed the existence of many intermediates and their interrelationships to provide a complete picture of the transformation, which can bring new inputs to a rational design of new photoactivatable pyronin or xanthene derivatives.

Introduction

The controlled heterolytic cleavage of nonpolar covalent bonds, such as a C–C bond, belongs among the most desired tasks in organic synthesis, although arduous conditions or transition-metal catalysis are usually required to make such reactions synthetically useful.[1,2] The photochemical homolytic cleavage of nonpolar covalent bonds is frequent in many primary photoinitiated processes,[3] whereas the photochemical heterolytic cleavage is less common.[4–6] Photochemical heterolysis of some common polar bonds may require a specific conical-intersection control to give destabilized carbocations in relation to the stabilized excited-state surfaces.[7] For example, the specific role of conical intersections could be used for explaining the "meta effect"[8] or the photochemical heterolysis of carbon-leaving group (C–LG) bonds in some photoactivatable systems (or photoremovable protecting groups, PPGs), which allow spatial and temporal control over the release of various molecules of interest.[9]

In the past decade, several novel visible-light-absorbing photoactivatable systems have been developed. The arguably first non-metal-based PPG absorbing over 500 nm, (6-hydroxy-3-oxo-3*H*-xanthen-9-yl)methyl group, was shown to undergo an intramolecular C–LG bond cleavage (Scheme 1a) upon irradiation with green light.[10] Later, several *meso*-methyl-BODIPY-based PPGs (Scheme 1b) have been designed to release LGs,[11–13] representing synthetically accessible and thermally stable scaffolds with structurally easily adjustable optical and photophysical properties. Many other transition-metal-free PPG systems have been reported to date.[14–19]

Irradiation of pyronin derivative **1**, analogous to (6-hydroxy-3-oxo-3*H*-xanthen-9-yl)methyl moiety (Scheme 1a), bearing a dithian-2-yl group in the C9-position, with visible light (λ_{irr} = 592 nm) was reported by some of us to exhibit a rather unexpected chemical transformation at the *meso*-methyl carbon atom.[20] The only observed intermediate was *meso*-methoxy pyronin derivative **2**, successively converted into 3,6-di(piper-

[a] Dr. M. Martínek, Dr. T. Slanina, Dr. L. Ludvíková, Prof. P. Klán
Department of Chemistry
Faculty of Science
Masaryk University
Kamenice 5, 625 00 Brno (Czech Republic)
E-mail: klan@sci.muni.cz
[b] Dr. M. Martínek, Dr. P. Šebej, Dr. T. Slanina, Dr. L. Ludvíková, Prof. P. Klán
RECETOX
Faculty of Science
Masaryk University
Kamenice 5, 625 00, Brno (Czech Republic)
[c] Dr. J. Váňa
Institute of Organic Chemistry and Technology
Faculty of Chemical Technology
University of Pardubice
Studentská 573, 532 10, Pardubice (Czech Republic)
[d] Dr. R. Navrátil
Department of Organic Chemistry
Faculty of Science
Charles University
Hlavova 2030/8, 128 43 Prague (Czech Republic)
[e] Prof. J. Roithová
Institute for Molecules and Materials
Radboud University
Heyendaalseweg 135, 6525 AJ Nijmegen (The Netherlands)
E-mail: j.roithova@science.ru.nl

Supporting information for this article is available on the WWW under https://doi.org/10.1002/cplu.202000370

This article is part of a Special Collection on "Chemistry in the Czech Republic".

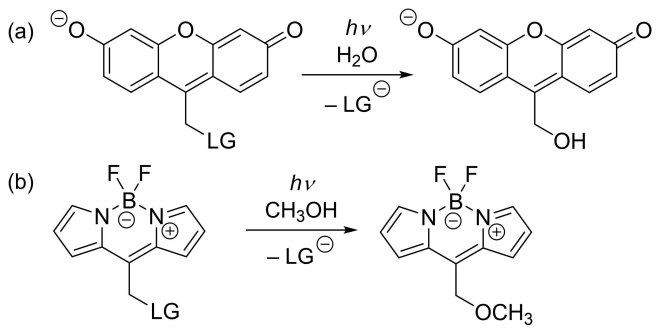

Scheme 1. Examples of recently developed visible light absorbing photoactivatable systems based on (a) (6-hydroxy-3-oxo-3*H*-xanthen-9-yl)methyl moiety and (b) *meso*-methyl-BODIPY core.[10,12]

idin-1′-yl)-9*H*-xanthen-9-one **3** as the final isolable product (Scheme 2). Although the mechanism of this phototransformation was not investigated in detail, it was suggested that a photoinduced electron transfer from an electron-rich sulfur atom to the electron-deficient pyronin core might be the first step followed by a nucleophilic attack of methanol as a solvent at the C9 position. Analogous photoinduced electron transfer from the dithiane moiety to an excited photosensitizer was demonstrated by Falvey, Kutateladze, and coworkers to be the key step in the fragmentation of dithiane-carbonyl adducts.[21,22] The second plausible explanation of the phototransformation of **1** is the release of an alkylthiolate as a LG (nucleofuge), similar to the reaction observed for PPGs shown in Scheme 1.

In this work, a thorough mechanistic study of the photochemistry of pyronin **1** using several advanced steady-state and transient spectroscopic and analytical techniques as well as quantum-chemical calculations is presented. Several short-lived intermediates were determined in the individual photochemical steps, and the roles of oxygen and solvent molecules in the reaction mechanism were established. Because the dithiane scaffold is a versatile protecting group for carbonyl compounds,[23–25] our study of the photochemistry of **1** can serve as an example of the mechanistic investigation of an extremely complex chemical transformation.

Results and Discussion

Photodegradation of the 9-dithianyl-pyronin derivative **1** is a complex reaction. Classical spectroscopy techniques allowed us to intercept one major intermediate (**2**, Scheme 2)[20] but at the same time, they indicated that the overall transformation is more complicated. In this paper, we first discuss the photophysical properties of reactants and major products, and then we demonstrate how optical, mass and NMR spectroscopies were used to identify and monitor different intermediates formed during the reaction. Finally, all data together with density functional theory (DFT) computations are used to unravel the reaction mechanisms.

Major Photoproducts

The photochemistry ($\lambda_{irr} = 592$ nm, Figure S55 in the Supporting Information) of **1** in methanol leads to the final major product, 3,6-diamino-9*H*-xanthen-9-one derivative **3** (>80% chemical yield, Scheme 2), which can be isolated.[20] The reaction proceeds further under exhaustive irradiation by white LEDs (3×100 W, Figure S58) resulting in the decomposition of molecule **3**. ^{1}H NMR analyses performed in this work revealed that the formation of **3** is accompanied by the formation of methyl formate (**4**, a signal at $\delta = 8.1$ ppm; Figures S60 and S63) as a co-product in up to ~60% chemical yield. The reaction was carried out in methanol, therefore, the initially formed compound could either be methyl formate or formic acid that reacts with methanol. Indeed, esterification takes place readily upon the addition of formic acid in methanol under identical conditions (Figure S76), however, it was impossible to prove or refute the intermediacy of formic acid due to overall low concentrations of intermediates during the irradiation experiments (typically $c(\mathbf{1}) \sim 10^{-5}$ mol dm^{-3}). We also searched for

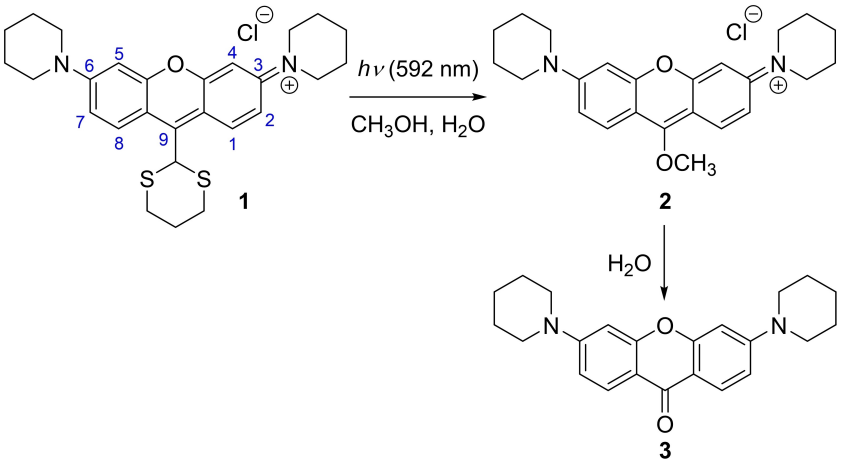

Scheme 2. Yellow-light induced transformation of pyronin-dithiane derivative **1**.

gaseous photoproducts using GC-MS headspace analysis, and we observed carbon monoxide (CO) evolution (~9% yield; CO was also identified by IR gas-phase spectroscopy and a reduction gas analyzer detector[26,27]). Experiments performed in $CH_3OH/D_2{}^{18}O$ (99:1, v/v) revealed that the ^{18}O isotope is incorporated into $C^{18}O$, suggesting that it occurred before the decarbonylation step took place.

Photophysical Properties of Compounds 1 and 3

Compound **1** exhibits a strong absorption at $\lambda_{max}(abs) = 585$ nm ($\varepsilon_{max} = 62000\ mol^{-1}\,dm^3\,cm^{-1}$) and 590 nm in methanol and water, respectively, and a relatively strong emission at $\lambda_{max}(em) = 608$ nm ($\Phi_f = (14.7 \pm 0.1)\%$;[20] $\tau_f = (1.35 \pm 0.02)$ ns) in methanol (Figure S22). The excitation spectra match the absorption spectra. The absorption spectrum of compound **1** in an aqueous solution ($c > 1 \times 10^{-5}\ mol\,dm^{-3}$) showing an additional band at 547 nm (Figure S23) suggests that the chromophore aggregates[28,29] due to its hydrophobic and relatively rigid structure. No aggregates were observed upon the addition of 10% of an organic co-solvent such as DMSO. The main product **3** (Scheme 2) features a major absorption band at $\lambda_{max}(abs) = 382$ nm ($\varepsilon_{max} = 33900\ mol^{-1}\,dm^3\,cm^{-1}$) and a strong emission band at $\lambda_{max}(em) = 448$ nm in methanol.[20] Compound **3** is not soluble in water even in the concentration range commonly used for absorption spectroscopy measurements (10^{-5}–$10^{-4}\ mol\,dm^{-3}$); the addition of water to methanol solutions of **3** leads to its precipitation.

Effects of Dioxygen

The major deactivation pathways of singlet-excited xanthene and pyronin dyes are fluorescence and radiationless decays.[30] Only derivatives bearing heavy atoms, such as rose bengal, undergo efficient intersystem crossing.[31,32] We performed a series of experiments in the presence of various triplet quenchers and sensitizers to determine the multiplicity of the productive excited state of **1**, that is, the species responsible for its initial photochemical step. The photodegradation efficiency of **1** in methanol was found to be dependent on the concentration of oxygen, which may act both as a triplet quencher and as an oxidant. Upon irradiation at $\lambda_{exc} = 592$ nm, the observed rate of disappearance of **1**, monitored by absorption spectroscopy, increased three-fold in a deoxygenated solution (3 freeze-pump-thaw cycles; $c_{oxygen} \ll 5.1 \times 10^{-8}\ mol\,dm^{-3}$) when compared to that found for an aerated solution (Table S1 in the Supporting Information), which implies that oxygen acts as a triplet state quencher. Because the reaction was not quenched completely even in samples purged with oxygen, we concluded that the lifetime of the productive triplet state was too short to compete with a bimolecular triplet energy transfer[9] or other alternative reaction pathways are available. To further verify the triplet-state origin of the major reaction step, a methanol solution of **1** ($c = 3 \times 10^{-5}\ mol\,dm^{-3}$) and xanthen-9-one **3** ($c = 3 \times 10^{-5}\ mol\,dm^{-3}$), used as a triplet sensitizer (xanthone: $\Phi_{ISC} \sim 1$),[33] was irradiated at $\lambda_{exc} = 375$ nm, the wavelength at which **3** absorbs >80% of light, resulting in an identical mixture of photoproducts (Figure S34). In more thoroughly degassed methanol (6 freeze-pump-thaw cycles), the degradation of **1** was slower by 1–2 orders of magnitude compared to that observed in aerated solutions. Besides that, products **2** or **3** were not formed (Figure S35). This suggests that there is at least one principal reaction step that critically relies on the presence of oxygen, such as Type I or II oxygenations.[34–36] We estimated that the molar amount of residual oxygen in this sample is lower than that of the starting material (see later for details). It was also found that the solution acidity increased upon exhaustive irradiation (the initial glass electrode readout of 6.5 dropped to 3.5), therefore, the course of the reaction could also be affected by a change in pH.

Time-Resolved Experiments

Femtosecond pump-probe experiments were carried out to characterize the major transients formed upon excitation of **1**. The transient spectra of **1** in methanol ($c = 5 \times 10^{-4}\ mol\,dm^{-3}$) were recorded using 100-fs steps up to a 10 ps delay after the pump pulse ($\lambda_{exc} = 280$ nm). Fitting with a single exponential decay resulted in the spectra of two species with $\lambda_{max} = 465$ nm (lifetime $\tau = (1.1 \pm 0.1)$ ns) and $\lambda_{max} = 425$ nm ($\tau \sim 3$ ns; Figure 1), which were assigned to the singlet (^{1}**1***) and triplet (^{3}**1***) excited states, respectively, because their spectral features were similar to those of analogous singlet- and triplet-excited Si-rhodamines or phenyl and thienyl rhodamines.[37–39]

The signal of ^{3}**1*** in methanol ($\lambda_{ex} = 266$ nm, $c(\mathbf{1}) = 1.3 \times 10^{-5}\ mol\,dm^{-3}$) was not detected within the resolution of our nanosecond laser flash photolysis setup (>5 ns), because the lifetime of ^{3}**1*** is too short (see above). Instead, a new long-lived

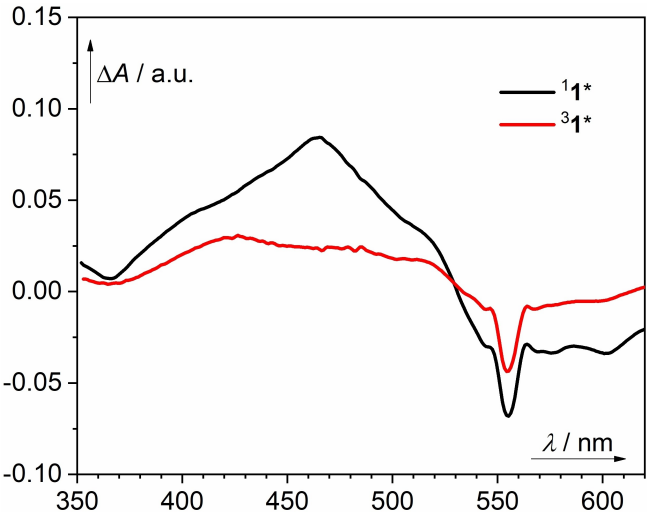

Figure 1. Deconvoluted excited-state absorption spectra of ^{1}**1*** (black line) and ^{3}**1*** (red line) resulting from a global analysis of the transient absorption spectra measured at short delays (0–10 ps) after the pump pulse ($\lambda_{exc} = 280$ nm) in methanol ($c(\mathbf{1}) = 5 \times 10^{-4}\ mol\,dm^{-3}$). Note: A broad negative band between 530 and 620 nm is the ground-state bleach of **1**; the peak at ~560 nm is an artefact from the laser pulse.

species (τ in the order of ms) was observed in the range of 560–600 nm, and it was attributed to the first, relatively long-lived intermediate formed directly from ^{3}**1***.

Detection and Assignment of Reaction Intermediates

Monitoring the **1**→**2**→**3** transformation by steady-state UV-vis spectroscopy suggested that the reactions are not elemental (Figure S24).[20] The spectra do not exhibit clear isosbestic points even at low concentrations of **1**. Thus, other intermediates were most likely formed in low concentrations, which hampered their immediate detection. Electrospray ionization mass spectrometry is an ideal tool to detect such low abundant species.[40–42] Hence, we irradiated methanol, methanol/water, and acetonitrile/water solutions of **1** and analyzed the detected ions (λ_{irr} = 592 nm, Figure 2).

The structures of all relevant ions were determined based on their IR characteristics and other supporting methods, such as collision-induced dissociation experiments or photofragmentation pattern.[43–46] For clarity of the following text, these assignments, except for one example, are discussed in the chapter "Going Deeper: The Structural Assignment of Detected Ions" in Experimental Section, and the remaining details are provided in Supporting Information.

The detected dominant signals corresponded to inherently charged species bearing a conjugated xanthene backbone as those of reactant **1** (*m/z* 465) and intermediate **2** (*m/z* 377). Charge-neutral molecules, such as **3**, could also be detected in their protonated forms (i.e., **3**H$^+$ at *m/z* 363), albeit as less intense signals. Besides, the *m/z* signals of several additional intermediates were observed (Figure 3; except formate **4**, see the text above). Their abundances varied depending on the reaction time and the type of solvent. For example, Figure 2 shows intense signals of intermediate **5** and weak signals of compounds **6**–**9**. Their structures were assigned based on collision-induced dissociation (CID) experiments (Figures S7 and S8),[43] isotopic labeling (Figures S9, S43, and S44), and infrared photodissociation spectroscopy (Figures S1–S4 in the Supporting Information).[44–46] At short photolysis times, we detected the first low-intensity signal at *m/z* 497 that corresponds to an adduct of **1** + 32 mass units. It was assigned either to an adduct of **1** with methanol (**6** or **7**) or a product of oxidation of **1**, such as sulfone **8**. Upon prolonged irradiation, major signals corresponding to **2** (*m/z* 377), **5** (*m/z* 407), and **9**H$^+$ (*m/z* 439) and minor signals assigned to **10** (*m/z* 347) and product **3**H$^+$ (*m/z* 363) were found. Upon irradiation of **1** in CH_3CN/H_2O (9:1, v/v), major signals corresponding to aldehyde **11** (*m/z* 375) and its hydrate **12** (*m/z* 393) were observed, whereas photolysis of **1** in CH_3OH/H_2O enabled the detection of intermediates **13** and **14**. Many of the detected species were formed by reactions of intermediates with methanol or water molecules, which was confirmed by performing the reactions in isotopically labeled solvents (see the *m/z* signal changes in Figure 3).

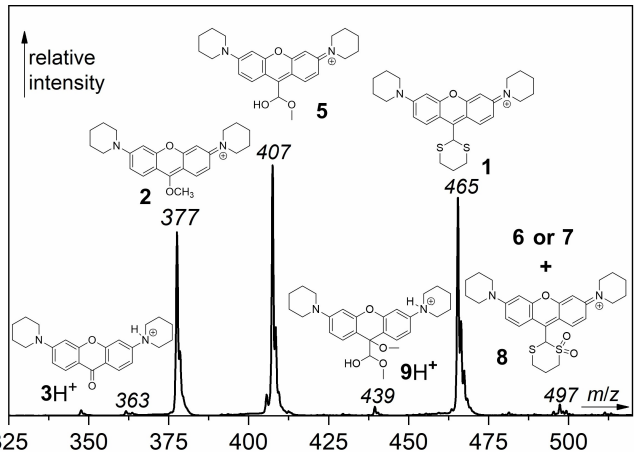

Figure 2. A representative MS spectrum collected after 1 h of irradiation of **1** ($c = 10^{-5}$ mol dm^{-3}) in methanol with LEDs (λ_{irr} = 592 nm, for the setup see Figures S54 and S55).

Structures of all ions were assigned based on their fragmentation patterns and based on their vibrational spectra (e.g., Figure 4, see also Supporting Information). We measured infrared spectra of mass selected ions by helium tagging photodissociation approach.[47] The experimental helium tagging infrared photodissociation (IRPD) spectra are usually well compared with theoretical IR spectra of ions in the gas phase allowing their assignment based on a comparison. One example is shown in Figure 4 where the experimental IRPD spectrum of ions at *m/z* 375 matches with the theoretical spectrum of aldehyde **11** allowing the assignment.

Having established the structures of the detected intermediates, we also investigated photofragmentation spectra of compounds **2**, **5**, **11**, **13**, and **14** in the visible part of the spectrum (430–700 nm).[48] Upon absorption of a photon, the mass-selected ions in the gas phase fragment. The absorption spectra of the mass-selected ions are determined from the yield of this photofragmentation as a function of the photon wavelength (Figures 5 and S2). The absorption band of isolated ion **1** was found hypsochromically shifted by ~40 nm compared to that of **1** in a methanol solution (Figure S2), and we expected to find similar media effects for all other investigated xanthene derivatives. Their absorption spectra at least partly overlap with that of **1**. Because the intermediates were formed during the course of irradiation, they could also be excited except for intermediate **2**, the spectrum of which is hypsochromically shifted outside the wavelength range of an irradiation source. Interestingly, the photofragmentation of **11**, **13**, and **14** in the gas phase resulted in decarbonylation; for example, carboxylate **13** gives directly the final product **3**, and methyl ester **14** photofragments to **2**. These phototransformations are unimolecular processes and do not reflect solvent effects. Therefore, they are only remotely useful for the interpretation of chemical processes occurring in protic solvents.

Furthermore, we investigated which intermediates are formed directly upon irradiation and which are formed in the subsequent dark processes (Figures S42 and S43). The photodegradation of **1** was found to correlate with the increase in signal intensities of methoxy intermediate **2**, hemiacetal **5**, and a methanol adduct of hemiacetal **9**H$^+$. These results showed that **9**H$^+$ is likely formed from **5** because the growth of the **9**H$^+$

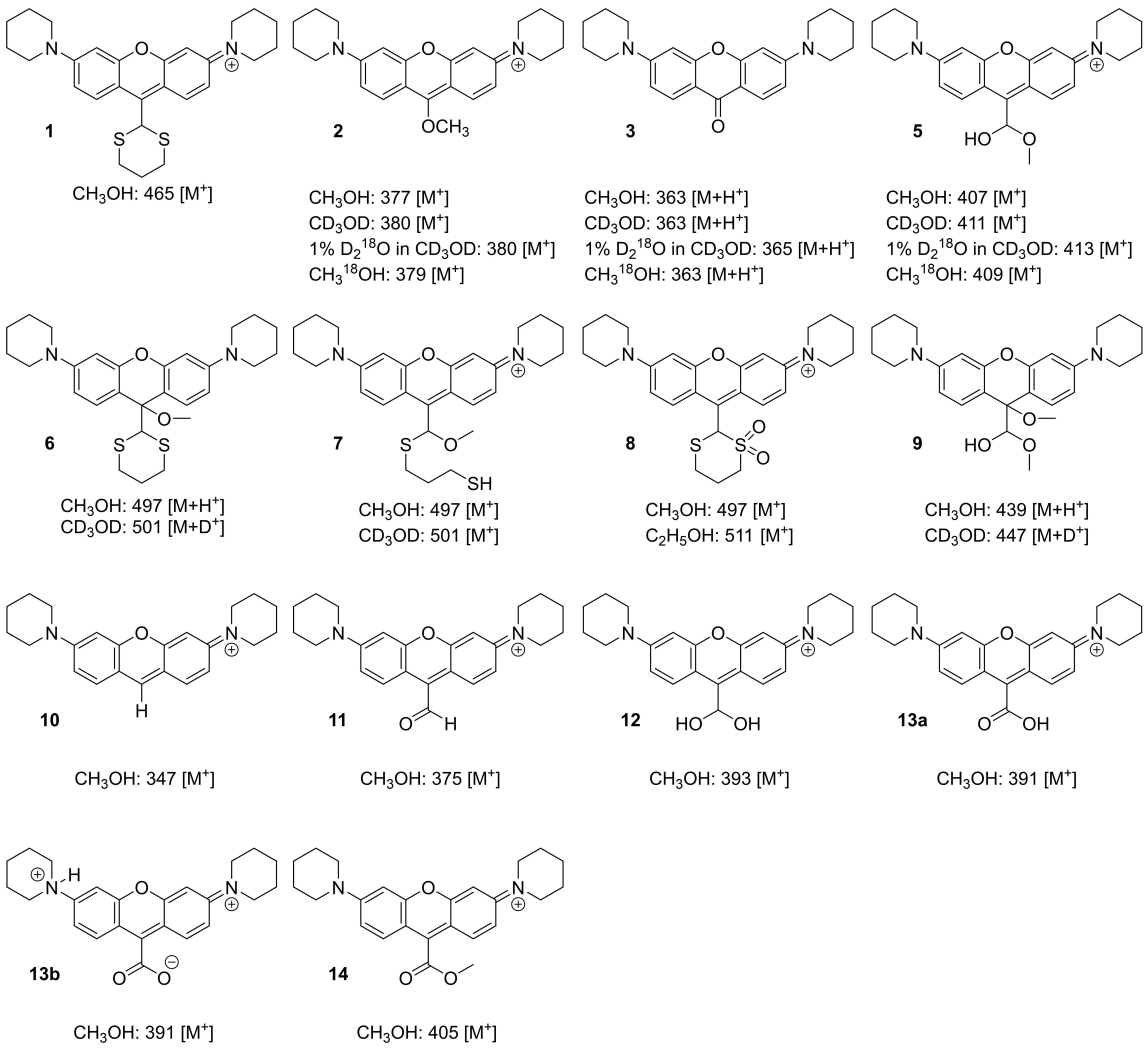

Figure 3. Species detected by electrospray ionization mass spectrometry upon irradiation of **1** in indicated solvents. The values refer to the corresponding *m/z* signals of intermediates in given isotopically labeled solvents.

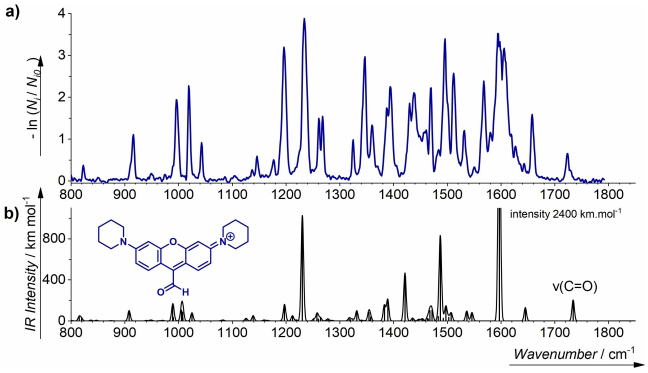

Figure 4. (a) Helium tagging IRPD spectrum of mass selected ion at *m/z* 375 measured at 3 K. (b) Theoretical infrared spectrum of **11** calculated at the B3LYP-D3/6-311 + G** level of theory. Theoretical vibrational frequencies were scaled by 0.975. Gaussian broadening (FWHM of 5 cm^{-1}) was applied to the theoretical infrared spectra for better comparison with the experimental infrared photodissociation spectra.

signal was always slightly delayed. The intensity of the signal at *m/z* 497, tentatively assigned above to an adduct of **1** with methanol (**6** or **7**) or sulfone **8**, formed by the oxidation of **1**, increased only initially and then slightly decreased during the first dark period (Figure S41). Compound **6** is most probably metastable and should not be responsible for a persistent signal, whereas intermediate **7** should react further upon irradiation (see later). Therefore, possibly photochemically less reactive sulfone **8** was assigned to the *m/z* 497 signal.

NMR Spectroscopy

The changes in concentrations of **1**–**5** and **7** upon irradiation of a CD_3OD solution of **1** in an NMR tube (containing a sealed capillary with an internal standard) by white LEDs (3×100 W; Figure S58) were analyzed by ^1H NMR spectroscopy to follow the reaction kinetics and to determine the interrelationships of the detected intermediates. The experiments were performed under argon, air, or oxygen atmosphere to study the effects of oxygen on the

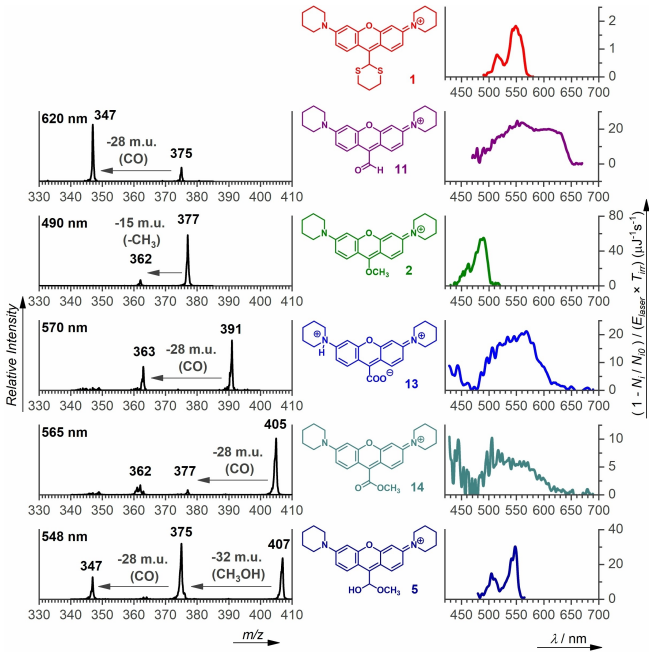

Figure 5. Visible photofragmentation spectra of indicated mass-selected ions (right), and the corresponding photofragmentation mass spectra at the indicated irradiation wavelength (left).

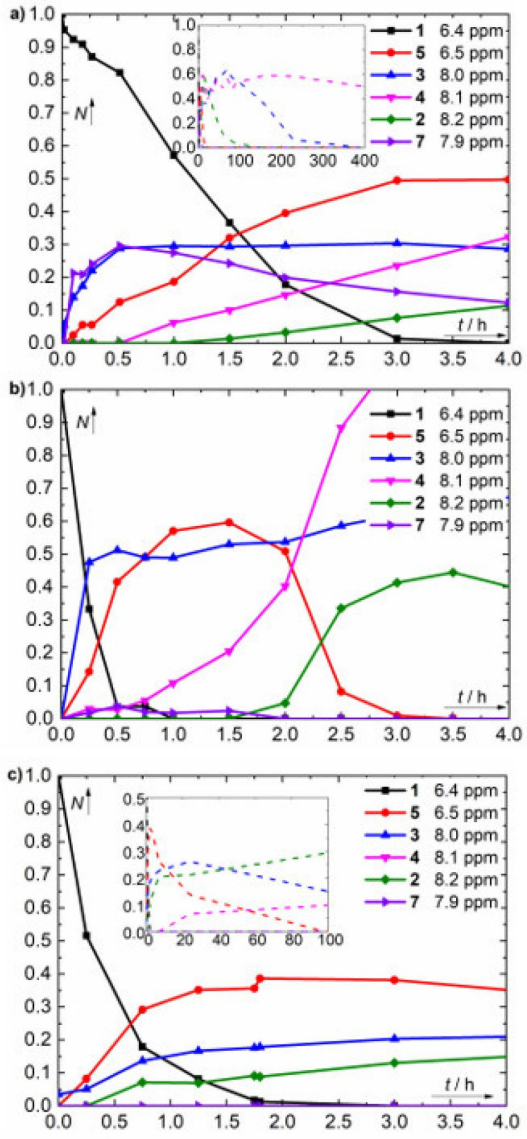

Figure 6. Time evolution of the integrated ^{1}H NMR signals in irradiated solutions of **1** in methanol-d_4 which were saturated with (a) air, (b) oxygen, and (c) argon (data points are connected with straight lines for clarity). The insets represent longer time scales.

individual reaction steps (Figures 6a–c). It should be emphasized that the concentrations of **1** in NMR experiments were two orders of magnitude higher ($c = 4 \times 10^{-3}$ mol dm^{-3}) than those used in MS and UV-vis ($c \sim 10^{-5}$) experiments described above. NMR analyses enabled a more reliable detection of two compounds, thioacetal **7** and ketone **3**, for which the mass spectrometry analysis was not sufficiently sensitive.

At first glance, the occurrence of all species detected by NMR (Figure 6a) was found in the following order: **1**→**7**→**5**→**2**. The final product **3** was formed already in the first minutes of irradiation, whereas formate **4** appeared later. The maximum chemical yields of intermediates **2** and **5** as well as final products **3** and **4** reached 60–65% in aerated solutions, that of **7** was ~30%. The only compound the concentration of which remained constant even upon exhaustive irradiation was **4**. The chemical yield of CO photoproduction (headspace GC/MS) was 8%.

The initial fast formation of **3** in aerated samples (ca. 30% yield maximum after 0.5 h; Figure 6a), attributed to direct oxidation of **1** and its dark decomposition to **3** (see later), is followed by the subsequent slower photochemical formation of **3** to give a maximum (~60%) yield after 70 h (see an inset of Figure 6a). In contrast, the yields up to 50% were observed in oxygen-purged samples (Figure 6b) after 0.5 h, however, no significant production of **3** was detected at longer irradiation times. In the case of argon-purged solutions (Figure 6c), only an inefficient formation of **3** occurred, and its kinetics was similar to that of the second (slow) process observed in oxygenated solutions.

The reaction kinetics in a solution saturated by oxygen was apparently faster (Figure 6b, the methanol solution was purged with oxygen, $c_{oxygen} = 10.2 \times 10^{-3}$ mol dm^{-3}).[49] A two-fold faster decomposition of **1** and the formation of **5** (and subsequently **2**) without significantly affecting the maximum chemical yields of both **5** and **2** (Figure 6b) may have a plausible explanation. Our experiments suggested thattriplet-excited compound **1** is quenched by oxygen only partially and the overall rate of the disappearance of **1** is much faster at higher O_2 concentrations, which implies that there is an alternative pathway for the conversion of **1** into **5**. The oxidation of sulfur of the dithiane moiety may result in the formation of sulfones (see analysis of the ions detected by ESI-MS), which could also be converted into common intermediate **5**. The synchronized formation of other intermediates follows the same order of appearances observed in Figure 6a. The formation of formate proceeded concomitantly with the production of **2** and preceded the formation of **3**. The chemical yield of CO (headspace GC/MS) was 9%.

Both the degradation of **1** and the formation of **5** in solutions of **1** purged with argon ($c_{oxygen} \sim 5.1 \times 10^{-8}$ mol dm^{-3}; Figure 6c) were faster compared to rates observed in aerated solutions. We hypothesized that it is related to the fact that the triplet-excited state of **1** is not fully quenched by oxygen and that oxygen is not required in the reaction leading to **5** (Figure 6c). The NMR signals of **5** were weaker and methoxy derivative **2** was formed faster than in aerated/oxygenated solutions (Figures 6a and 6b). We thus imply that the excited state of **5** preceding the formation of **2** is also a triplet. Lower overall maximum yields of intermediates **2** and especially **3** suggest that oxygen also acts as an oxidant during their formation. The oxygen level in argon-purged samples might be low enough to preclude quenching of the triplet states but still large enough (1 equiv. at least) to oxidize the intermediates. Formate **4** was not initially formed in the absence of oxygen. The chemical yield (headspace GC/MS) of CO was slightly higher (13%) compared to those of aerated and oxygenated samples (8%).

We paid a special attention to the formation of aldehyde **11** as the last identified intermediate on the pathway leading to **2**, particularly because NMR experiments did not provide any evidence of its presence in the spectral region typical for aldehydes. On the other hand, the formation of **11** and its hydrate **12** was unambiguously detected by ESI-MS, particularly in the mixture of CH_3CN/H_2O (9:1, v/v; Figure S9).

Mechanism

We identified major intermediates (MS) and monitored their concentrations (NMR) in the course the photoreaction of **1** carried out under various conditions. Our experiments suggested the order of their appearances, **1**→**7**→**5**(→**11**)→**2**, and their maximum concentrations and the absence of other (photo)products gave us the first evidence about their interrelationships. Scheme 3 shows the proposed overall mechanism based on the results from all experimental and computational studies. The scheme depicts structures of intermediates detected by our analytical methods (black), plausible short-lived species (red), and possible but undetected intermediates (blue).

The first reaction step of triplet excited ^{3}**1***[39,50,51] is the C–S bond heterolytic cleavage resulting in the dithiane ring opening. The formation of a carbocation intermediate followed by the nucleophilic attack of a solvent, such as methanol, to give **7** would be a plausible pathway analogous to the reactions observed for *meso*-methyl BODIPY[11–13] or xanthene[10] derivatives (Scheme 1). The concentration of intermediate **7** was always found to be very low, suggesting that the photochemical efficiency of its subsequent photodegradation is very high. If undetected hemithioacetal **15** is formed in the presence (or traces) of water instead, it must be promptly converted into a different species, such as **5** or **9**. Indeed, the hydrolysis of hemithioacetals is known to be diffusion-controlled under acid or base catalysis.[52,53] Thiolate as conjugate base of a moderately strong acid is a mediocre leaving group (although better than alcoholates), which can be liberated, for example, from a 4-hydroxyphenacyl PPG upon irradiation.[54] The photochemical opening of 1,3-dioxolane rings attached to 4-coumarinyl[55] or 2-(2-hydroxy-4-methoxyphenyl)[56] cages has also been reported. However, the former study showed that six-membered 4-coumarinyl-1,3-dioxanes are photochemically inert because of the inherently higher thermodynamic stability of a six-membered ring.[55]

The presence of oxygen in solution partially quenches the triplet state ^{3}**1***, but higher concentrations of dissolved O_2 lead to dithiane oxidation. The oxidation products may undergo further reactions or eventually give the same final product **3**. Cationic pyronin chromophores, such as **1**, are known to be in equilibrium with neutral xanthydrol **16** in the presence of water[57] (Scheme 4) or with their methoxy analogs in methanol. Only some of them were detected by our analytical techniques (*e.g.*, **6**, **9**, **17**). The absorption spectra of such species are largely hypsochromically shifted ($\lambda_{max} \sim 460$ nm),[57] thus they cannot be directly excited at the irradiation wavelength used in our experiments. The equilibrium constant for pyronin-based (=P) xanthydrol **16** ([POH]/[P$^+$][OH$^-$]) of -2.6[57] suggests that their participation in any chemical transformation is minimal. This was evidenced in an experiment, in which the light source was periodically turned off and on (Figure S41). The intensities of the MS signals of major intermediates **11**, **7**, **5** remained constant during the light-off phase, therefore, their transformations were initiated photochemically.

In contrast, the changes in the signal intensities of intermediates lacking the xanthene-core conjugation, such as **6**, **9**, and **17** (Figure S41), were found photochemically inert. The photochemistry of **1** in methanol solution containing furfurylalcohol (0.1%vol.) provided no evidence of the presence of singlet oxygen trapping products. Therefore, we suggest that the formation of singlet oxygen is negligible and does not interfere with the reaction course. Cyclic thioethers readily undergo single-electron-transfer oxidation due to their low oxidation potential, which was utilized in the photochemical ring-opening of 1,3-dithiane to give carbonyl compounds in the presence of oxygen via dithianyl radical cation intermediates.[58–60] Such a radical cation undergoes either single-electron transfer to form dithioacetal dication to trigger the C–S bond cleavage and subsequent hydrolysis to give ketone,[61] or it can be attacked by air oxygen or superoxide radical anion to form persulfides.[58,62] Dithiane oxidation was a significant pathway observed only in oxygen saturated solutions, however, we observed no EPR signal in the irradiated mixtures (see Supporting Information for more details), thus we have not further investigated this process.

Additional photon is needed for the phototransformation of **7** into hemiacetal **5**, which is analogous to the conversion of ^{3}**1*** into **10**. Compound **5** was always observed as one of the principal intermediates and its maximum concentration typically reached 60% (NMR). Its further transformation to hydrate **12**, which is in equilibrium with aldehyde **11**, evidently took place via the triplet excited state (see quenching with oxygen above; Scheme 3), but we should also not exclude a dark hydrolysis as a minor pathway.

The most difficult part of this investigation was to clarify the mechanism of the conversion of **11** to **2** (and subsequently **3**).

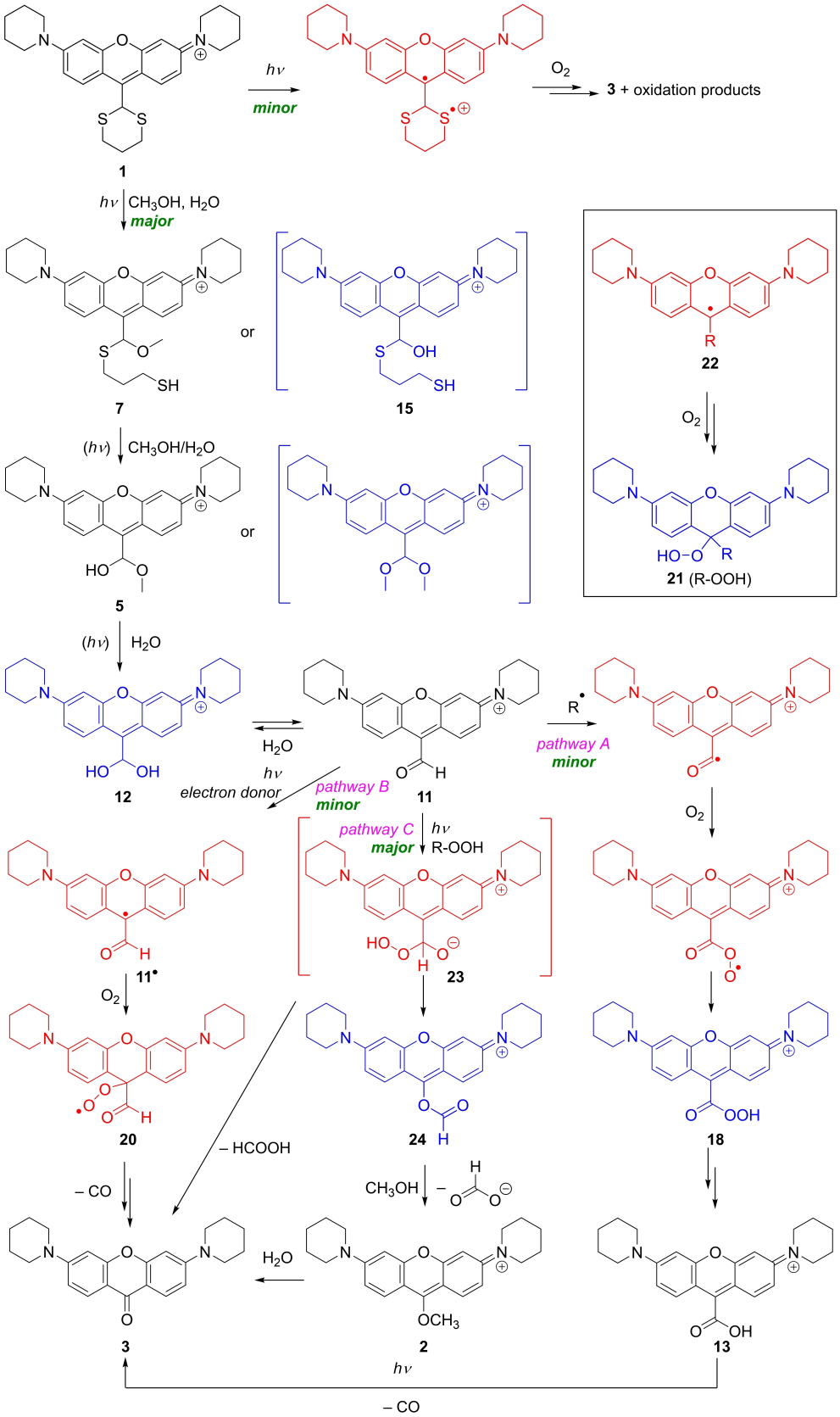

Scheme 3. The proposed mechanism of the phototransformation of **1** in a methanol/water mixture, showing the intermediates detected by our analytical methods (black), plausible short-lived species (red), and possible but undetected intermediates (blue).

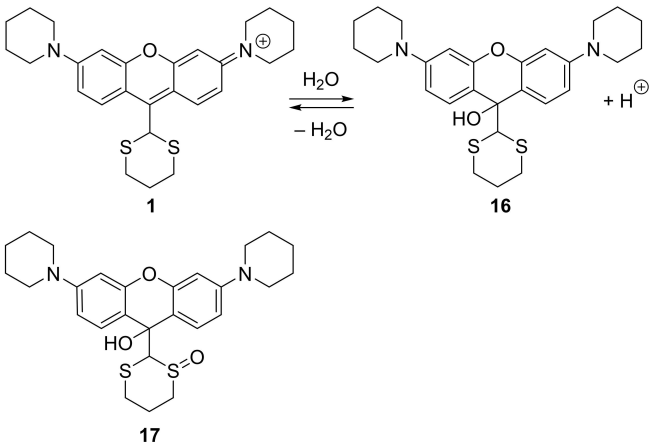

Scheme 4. Equilibrium between **1** and its corresponding xanthydrol **16** in an aqueous solution, and **17** as the product of oxidation of **1** or **16**.

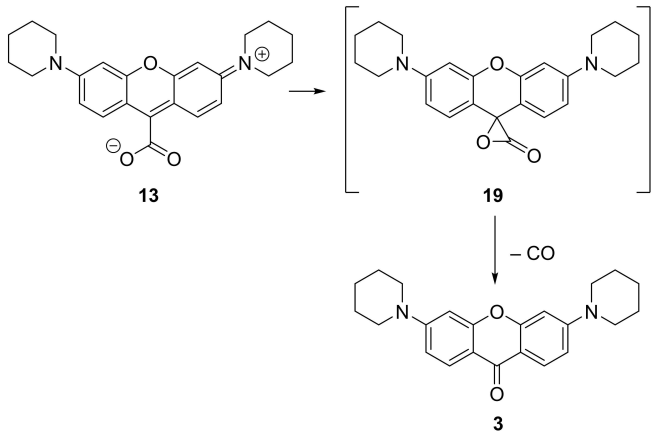

Scheme 5. Formation of a putative α-lactone intermediate **19** and subsequent CO liberation.

This transformation involves bond umpolung, requires the presence of oxygen, and consists of several steps (Figure S12). However, we were not able to detect any additional associated intermediates. The C–C bond is cleaved and the overall reaction is oxidation. Oxygen (O_2) has a dual effect on the reaction; it slows down some of the individual reaction steps but is required as a reactant (oxidant). We proposed nine possible reaction mechanisms for this transformation (Figures S12–S21). Quantum chemical calculations at the M06L-D3/def2TZVP PCM (MeOH) level of theory[63–66] allowed us to rule out five proposed mechanisms and one was excluded based on the absence of suggested photoproducts (Supporting Information).

Finally, the three remaining plausible reaction mechanisms of the formation of **2** from aldehyde **11** are: (A) the formation of pyronin-9-carboxylic acid **13** via oxidation of aldehyde **11** and its photochemical conversion to **3**, (B) a single-electron reduction of **11** and subsequent oxidation, and (C) a solvent-assisted Dakin-like reaction[67] to give **2** as the key intermediate on the way to **3** (Scheme 3).

In *pathway A*, carboxylic acid **13** could simply be formed by a dark autoxidation of aldehyde **11** in the presence of oxygen[68,69] via radical photoinitiation (Scheme 3).[70] The resulting acyl radical could efficiently couple with ground-state oxygen to form peroxy acid **18**,[71,72] which would react with another molecule of aldehyde and rearrange to give a Criegee-like intermediate, which disproportionates into two molecules of acid **13**.[73,74] Our previous work suggested that pyronin-9-carboxylates, analogous to xanthene-9-carboxylic acid,[75] could release carbon monoxide (CO) upon irradiation via a putative α-lactone intermediate (**19**, Scheme 5), observed, for example, in atmospheric photochemistry of methacrolein.[76,77] Another example is the 9-acridinecarboxaldehyde oxidation to give 9-acridinecarboxylic acid and 9(10*H*)-acridinone, observed as a minor byproduct.[78]

Although CO was detected as a reaction side-product in less than 10% yield, we searched for the presence of carboxylic acid **13** and its methyl ester **14** in irradiated samples by ESI-MS. Small amounts of both compounds were detected upon irradiation of **1** in methanol, and thus they were synthesized independently to elucidate their roles in the reaction mechanism (Scheme S2). Upon the irradiation of **13** and **14** under the reaction conditions identical to those used in the photolysis of **1**, their photodegradation quantum efficiency was at least 100 times lower than that of **1** (Figures S38 and S40). The compounds were almost unreactive even in the mixture with other intermediates formed upon irradiation of a solution of **1** (Figure S39). Therefore, we excluded both **13** and **14** as key intermediates of the **11**→**3** reaction; their contribution as a source of CO has to be insignificant. Direct photodecarbonylation of aldehyde **11** was also considered but this hypothesis suffered from two drawbacks. The formation of C9 radical was found to be endothermic by 50 kcal mol^{-1} (M06L-D3/def2TZVP, PCM (MeOH); Figure S19), and the transition-state energy of the CO dissociation via the direct homolytic C–C bond cleavage should also be very high as we could not localize the transition state in our DFT calculations. However, the products are ~89 kcal mol^{-1} higher in energy than aldehyde **11**; Figure S20). In addition, the direct decarbonylation of **11** should give pyronin **10** formed by the reduction of pyronin C9 radical (Figure S19). Because **10**[79] is unreactive under the given conditions as evidenced by the photolysis of an authentic sample of **10** by 592-nm light in this work, it should accumulate in the reaction mixture, which was not observed. Therefore, the decarbonylation of **11** was rejected as the major pathway.

The second plausible reaction, *pathway B*, involves pyronin-9-peroxyradical-9-carbaldehyde **20** as the key intermediate and starts with the photoreduction of the triplet excited state of electron-deficient aldehyde **11** in the presence of an electron donor (Scheme 3), such as a sulfur-containing dithiane fragment, observed in structurally similar rhodamines.[80,81] The reaction gives pyronin **11**$^{\bullet}$ and thiyl radicals.[82] Intermediate **11**$^{\bullet}$ could react with triplet ground-state oxygen to form **20**,[83] which would further fragment to an acyl radical[84] and CO. An analogous reaction was proposed for methacrolein undergoing oxidation with atmospheric oxygen.[76,77] This pathway is the most probable decarbonylation step, although it is still a minor process in the overall reaction.

The most important evidence in our investigation was that methyl formate (as we demonstrated above, formic acid can be rapidly esterified in methanol) was produced in high chemical yields (~60%) along with high amounts of successive methoxy intermediate **2** and ketone **3**. We propose that the third reaction mechanism of the **11**→**3** transformation involves a water- or methanol-assisted Dakin-like reaction in the presence of oxygen (*pathway C*, Scheme 3).[67] The original Dakin method uses an excess of hydrogen peroxide and sodium hydroxide at elevated temperatures. Interestingly, flavin also catalyzes Dakin oxidation of aromatic aldehydes in the presence of oxygen or hydrogen peroxide as sacrificial oxidants under mild conditions.[85,86]

These examples have led us to suggest the most plausible mechanism of this reaction sequence. A tentative 9-hydroperoxy intermediate (**21**), formed by the reaction of pyronin radical **22** with oxygen (O_2) and an H-atom source with a weak C–H bond ([H]), such as thiols formed upon dithiane ring opening (Scheme 3), at the *meso*-carbon, can undergo a direct dissociation to give product **3** and formic acid (pathway *Ca*, Scheme 6; note that energies are given relative to the energy of **23**) with an activation energy of 22.8 kcal mol^{-1} (green lines; Figure S15). Alternatively, **21** can rearrange to form peroxy anion **23**, which lies 7.5 kcal mol^{-1} higher in energy than **21**. The structure of this hydroperoxy intermediate **23** has not been determined experimentally (either NMR or ESI-MS) in this work, although it figures as the key reactant in three reaction pathways. It can undergo a 1,2-aryl migration (*pathway Cb*, Scheme 6) to give an undetected 9-formyloxypyronin **24** in a Dakin-like process, a hydrogen migration (*pathway Cc*) to form carboxylic acid **13** or a proton shuttle via **25** to produce dioxetane **26** (*pathway Cd*, Scheme 6). All these reaction pathways possess very similar activation energies. *Pathways Cb* and *Cc* require the participation of a protic solvent molecule in the transition state (*e.g.*, water or methanol; the energies in Scheme 6 are calculated with a methanol assistance). The hydrogen migration (*pathway Cc*) is slightly energetically preferred to the Dakin rearrangement (*Cb*; Figure S15). *Pathway*

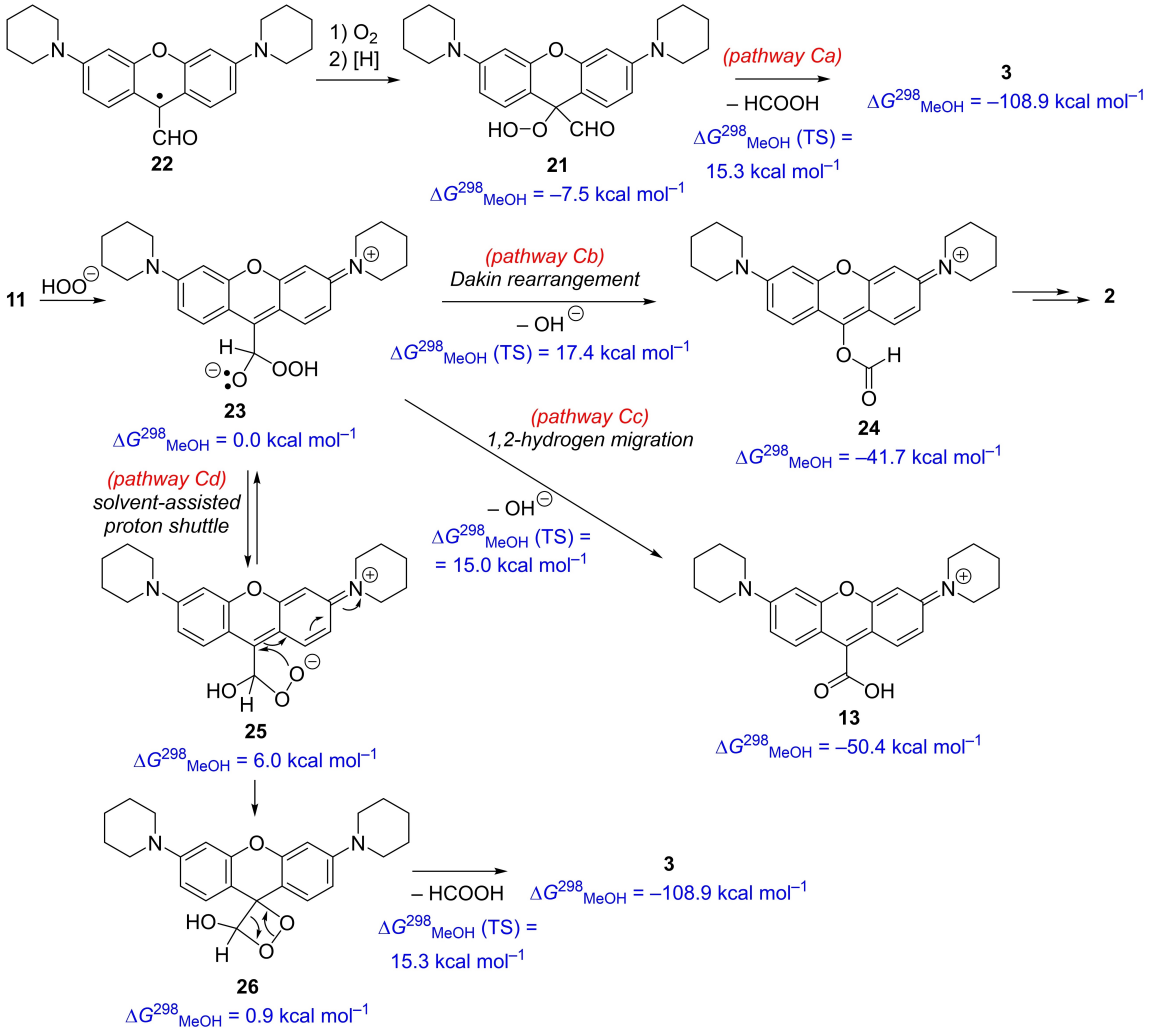

Scheme 6. The formation of 9-hydroperoxy intermediate **21** followed by: (Ca) the direct rearrangement of **21** into **3** and formic acid, (Cb) Dakin-like reaction of aldehyde **11**, (Cc) 1,2-hydrogen migration leading to acid **13**, and (Cd) the formation of dioxetane **26**. The Gibbs energies of the corresponding structures and transition states were calculated at 298 K in methanol solution (see also Figure S15) and are given relative to the energy of **23** ($G^{298}_{MeOH} = -951.054599$ Hartree).

Cd involving dioxetane **26** and leading to product **3** proceeds with the same activation energy as that of *Cc*. A stepwise Dakin-like dissociation to give formyloxy intermediate **24** must be assisted by a proton-shuttle molecule, such as protic methanol or water. The calculated relative energies of the corresponding intermediates and transition states were found to be close to each other (within ~2 kcal mol^{-1}) for methanol- and water-assisted pathways (Figure S15).

The nucleophilic substitution of the formyloxy group at the C9 position in **24** with methanol results in the formation of methoxypyronin **2**.[20] Both S_N1-like or addition-elimination mechanisms are possible. Intermediate **2** was found as one of the most persistent intermediates, the concentration of which reached ~40% yield (^{1}H NMR) in a typical reaction setup. Finally, **2** is slowly converted into ketone **3** in the presence of water, even in the absence of light, as reported before.[20]

Conclusions

This paper presents a thorough mechanistic study of the photochemistry of 9-dithianyl-pyronin **1** in methanol using advanced steady-state and transient spectroscopic and analytical techniques as well as quantum-chemical calculations. Several photoreactive intermediates were determined, and the roles of dioxygen and nucleophilic protic solvents in the reaction mechanism were established. The photoreaction was shown to proceed through pyronin-9-carbaldehyde **11** as the key intermediate and we suggested three plausible pathways for its conversion to the final photoproducts, xanthen-9-one derivative **3** and formate **4**: (A) the formation of pyronin-9-carboxylic acid **13** via oxidation of aldehyde **11** and its photochemical conversion into xanthen-9-one **3**, (B) single-electron reduction of **11** and its subsequent oxidation, and (C) either the direct dissociation of oxidized intermediate to formic acid and xanthen-9-one **3** or a solvent-assisted Dakin-like reaction to give methoxy derivative **2** as an intermediate on the way to **3**. The photochemistry of compound **1** induced by visible-light irradiation at 592 nm in the presence of oxygen involves several redox processes and a C–C bond cleavage (~80–90 kcal mol^{-1}).[87] Despite the complexity of the overall mechanism, we show that although the xanthen-9-yl moiety is not a suitable photolabile protecting group for aldehydes in this particular case, our mechanistic investigations provided many useful and sometimes surprising insights into the (photo) reactivity of substituted xanthene/pyronin dyes, the photobleaching of which can be a serious obstacle in their applications.

Experimental Section

Detailed Information on the Structural Assignment of Detected Ions

Ion at *m/z* 497 (Figure 3): The first intermediate on the degradation pathway of **1** is the ion at *m/z* 497. This ion is detected right in the beginning of the reaction. Formally, it can be formed by addition of methanol or two oxygen atoms to **1**. If the reaction proceeds in ethanol, CD_3OD or propan-2-ol, we observed a mass shift of these adducts to *m/z* 511, *m/z* 501, and *m/z* 525, respectively, confirming the reaction with an alcohol. However, the signal at *m/z* 497 was also present and its intensity remained relatively constant during the whole course of irradiation. Collision-induced dissociation of ions at *m/z* 497 showed a dominant elimination pathway of 64 mass units, which correspond to SO_2 (Figure S7). Therefore, the structure of this ion most probably corresponds to oxidized **1** with one sulfide group transformed to sulfone **8**.[20] Ions appearing in the beginning of the reaction corresponding to the adduct with alcohol could either be the products of an attack of methanolate at the C9-carbon atom of xanthene forming **6** (detected as protonated ions; this species should be photochemically inactive)[88] or a product of the ring opening (**7**).[20] Either **6**H$^+$ or **7** appear at low abundances for a short reaction time, therefore, we could not further characterize them.

Ion at *m/z* 407 (Figure 3): The signal at *m/z* 407 corresponds to hemiacetal **5** (Figure 2). The assignment was based on the agreement of the infrared photodissociation spectrum of this ion and the calculated IR spectrum of **5** (Figure S48). Further evidence for the structural assignment of **5** was based on the results from irradiation experiments performed in methanol-d_4 or $D_2{}^{18}O$ ($CH_3CN/D_2{}^{18}O$ mixture, 99:1, v/v), in which the corresponding MS signals of deuterium- and ^{18}O-labeled structures, respectively, were detected (Figures 3 and S9). The main dissociation pathway of **5** under CID conditions was found to be the loss of methanol (32 mass units, Figure S7) with the concomitant formation of a new species at *m/z* 375 (later assigned to aldehyde **11**, Figure 4). Similarly, **1**-*d* yields **5**-*d* (*m/z* 408) upon irradiation and **5**-*d* loses methanol (32 mass units, Figure S10) in CID to form aldehyde **11**-*d* (*m/z* 376). The aldehyde **11**-*d* loses CO in the MS experiment to form 9-(^{2}H)-pyronin **10**-*d* (*m/z* 348, Figure S10). In addition, the photolysis of **1** in $CH_3{}^{18}OH$ gave the expected analogous species at *m/z* 409, whereas the irradiation of **1** in ethanol and propan-2-ol led to the formation of analogous intermediates at *m/z* 421 and 435, respectively. Finally, the photolysis of **1** in CD_3OD gives the ion at *m/z* 411 that undergoes equilibration after dilution of the mixture with CH_3OH (Figure S44). We also analyzed the ^{1}H–^{13}C HSQC NMR spectra of **1** irradiated in CD_3OD, and the observed ^{1}H signal at $\delta =$ 6.47 ppm (HO–C**H**R–OCH_3, R = pyronin; Figure S64) was correlated with the ^{13}C signal at $\delta = 93.5$ ppm (HO–**C**HR–OCH_3; Figure S64); both signals are in the typical range expected for hemiacetals. The maximum chemical yield of **5** was ~60% (based on a quantitative NMR analysis).

Ion at *m/z* 391 (Figure 3): These ions correspond to either carboxylic acid **13** or formyloxy intermediate **24**. Two isomers of **13**, carboxylic acid **13a** and zwitterion **13b**, which could exist as an α-lactone (see Scheme 5), can be proposed (Figure 7). Helium tagging infrared photodissociation (IRPD) spectrum of this ion (*m/z* 391) does not show any bands in the range of 1700–2000 cm^{-1}. The lack of a clear carbonyl stretching band suggests that the detected ions do neither correspond to zwitterion **13b** nor to formyloxy intermediate **24**. Also, all other ions studied by IRPD spectroscopy (Figures 5, S2, and S3) have a conjugated xanthene backbone, which gives well-resolved spectra in the 1400–1700 cm^{-1} range.[89] Here, the spectrum is more convoluted which can be associated with the protonation of one of the piperidine moieties. Hence, the IRPD spectrum represents ion **13** in the form of zwitterion **13b**. Zwitterions in the gas phase lie considerably higher in energy than their neutral forms (see the relative energies in Figure 7); however, it has been reported earlier that protic solvents support electrospray ionization transfer of solution-favored protonated forms.[90] Ion **13** predominantly eliminates CO in the collision-induced dissociation, followed by the CO_2 elimination. This is again consistent with the structure of zwitterion **13b**.

Ion at *m/z* 375 and *m/z* 393 (Figure 3): Species at *m/z* 375 and *m/z* 393 were detected upon irradiation of **1** in a CH_3CN/H_2O mixture,

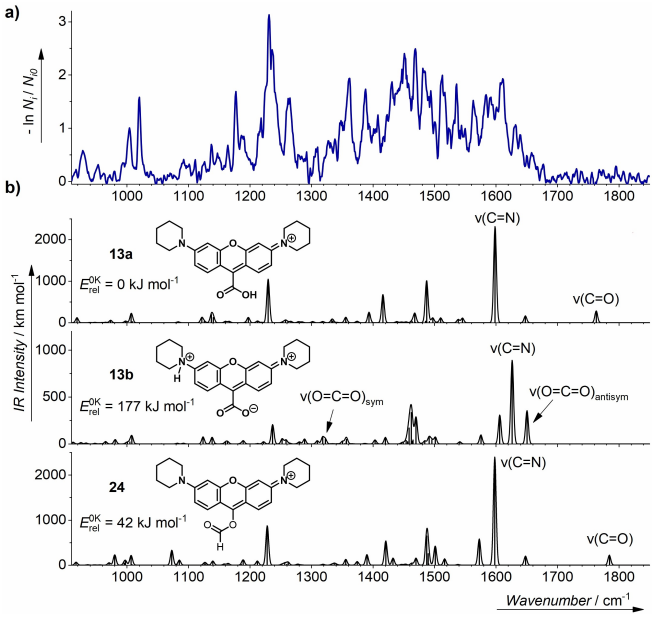

Figure 7. (a) Helium tagging infrared photodissociation spectrum of mass-selected ions at *m/z* 391. (b) Theoretical infrared spectra of carboxylic acid **13a**, its zwitterion **13b**, and formyloxy derivative **24** calculated at the B3LYP-D3/6-311 + G** level of theory. Theoretical vibrational frequencies were scaled by 0.975. Gaussian broadening (FWHM of 5 cm^{-1}) was applied to the theoretical infrared spectra for better comparison with the experimental infrared photodissociation spectra.

and we assigned them to pyronin-9-carbaldehyde **11** and pyronin-9-yl dihydrate **12**, respectively (Figure 3). We did not detect these species in a methanolic solution with low water content, most likely because the equilibrium between **8** and **11** and their corresponding methoxy hemiacetals and acetals was shifted strongly toward the latter. The IRPD spectrum of the ion at *m/z* 375 is in close agreement with the calculated IR spectrum of **11** (Figure 4). The CID spectrum shows the elimination of CO to form ions at *m/z* 347, presumably 9-*H*-pyronin **10** (Figure S8). We have also detected a hydrate of **11**, ion **12** (*m/z* 393). Hydrate **12** loses a molecule of water upon collisions to form **11**.

Ion at *m/z* 439 (Figure 3): The intermediate at *m/z* 439 was assigned to an adduct of **5** and methanol, **9** (Figure 3), based on the agreement of its IRMPD spectrum with the calculated one (Figure S45). The experiments performed under the same conditions in CD_3OD provided the ion at *m/z* 447, whereas an analogous adduct at *m/z* 469 was found in ethanol and the ion at *m/z* 440 upon irradiation of **1**-*d* in methanol. We did not observe any distinct NMR signals of these species; however, the reaction pathway might be different under different experimental conditions. Because the concentration of the starting material **1** was about two orders of magnitude higher in NMR experiment solutions, the probability of bimolecular processes is much higher but, at the same time, an internal optical filter effect is more pronounced.

Ion at *m/z* 377 (Figure 3): The ion at *m/z* 377 was previously assigned to 9-methoxy pyronin **2**,[20] the longest-lived intermediate observed in the UV-vis spectra. Upon irradiation of **1** in CD_3OD and $CH_3{}^{18}OH$, the signal at *m/z* 377 mass-shifted to *m/z* 380 and 379, respectively (Figure 3). In ethanol, an analogous species at *m/z* 391 was observed. No incorporation of ^{18}O into the molecule of **2** was observed when **1** was irradiated in a $CH_3CN/D_2{}^{18}O$ solution. The OCD_3 group in this intermediate, which was generated in CD_3OD, was exchanged for the OCH_3 group after dilution of the solution with CH_3OH (Figure S43). The main dissociation pathway in CID and in the photodissociation spectrum is the loss of the methyl group (Figure S7 and Figure 4, respectively). The IRPD spectrum provided a good agreement with the predicted one (Figure S50). We also assigned the ^1H NMR signals at $\delta = 8.2$ ppm to two aromatic hydrogens which are spatially closest to those of the methoxy group (Figure S63) and we estimated the yield of its formation (50 %, ^1H NMR).

Acknowledgements

Support for this work was provided by the Czech Science Foundation (GA18-12477S). We also thank the CETOCOEN EXCELLENCE Teaming 2 project (supported by the Czech Ministry of Education, Youth and Sports: CZ.02.1.01/0.0/0.0/17_043/0009632 and EU H2020: 857560) and the RECETOX research infrastructure (LM2018121) (P.K.). The results from the CLIO were obtained thanks to the funding from the European Union's Seventh Framework Programme (FP7/2007-2013) under the grant agreement No. 226716 (J. R.). The CLIO staff, particularly Vincent Steinmetz, is acknowledged for their help and assistance. In addition, we would like to thank Jiří Huzlík (CDV, v.v.i., Brno), Zdeněk Moravec (Masaryk University) and Lucie Muchová for consultations on the quantification of CO, Juraj Jašík for his help with ISORI MS experiments and technical assistance (both from the Charles University, Prague), Ján Tarábek (IOCB, Prague) for EPR analysis. We would also like to acknowledge Tatsiana Rusina and Branislav Vrana for the head-space GC-MS analysis, Miroslava Bittová for the HRMS analysis, Peter Horváth for the measurement of fluorescence quantum yield and Luboš Jílek (all from Masaryk University) for his assistance with light sources.

Conflict of Interest

The authors declare no conflict of interest.

Keywords: DFT calculations · dyes/pigments · photochemistry · reaction mechanisms · spectroscopy

[1] C.-H. Jun, *Chem. Soc. Rev.* **2004**, *33*, 610–618.
[2] K. Ruhland, *Eur. J. Org. Chem.* **2012**, *2012*, 2683–2706.
[3] P. Klán, J. Wirz, *Photochemistry of organic compounds: From concepts to practice*, 1st ed., John Wiley & Sons Ltd.: Chichester **2009**.
[4] P. Wan, S. Muralidharan, *J. Am. Chem. Soc.* **1988**, *110*, 4336–4345.
[5] P. K. Das, *Chem. Rev.* **1993**, *93*, 119–144.
[6] M. Freccero, M. Fagnoni, A. Albini, *J. Am. Chem. Soc.* **2003**, *125*, 13182–13190.
[7] A. T. Buck, C. L. Beck, A. H. Winter, *J. Am. Chem. Soc.* **2014**, *136*, 8933–8940.
[8] H. E. Zimmerman, *J. Am. Chem. Soc.* **1995**, *117*, 8988–8991.
[9] P. Klán, T. Šolomek, C. G. Bochet, A. Blanc, R. Givens, M. Rubina, V. Popik, A. Kostikov, J. Wirz, *Chem. Rev.* **2012**, *113*, 119–191.
[10] P. Šebej, J. Wintner, P. Müller, T. Slanina, J. Al Anshori, L. A. P. Antony, P. Klán, J. Wirz, *J. Org. Chem.* **2012**, *78*, 1833–1843.
[11] E. Palao, T. Slanina, L. Muchová, T. Šolomek, L. Vítek, P. Klán, *J. Am. Chem. Soc.* **2015**, *138*, 126–133.
[12] T. Slanina, P. Shrestha, E. Palao, D. Kand, J. A. Peterson, A. S. Dutton, N. Rubinstein, R. Weinstain, A. H. Winter, P. Klán, *J. Am. Chem. Soc.* **2017**, *139*, 15168–15175.

[13] J. A. Peterson, C. Wijesooriya, E. J. Gehrmann, K. M. Mahoney, P. P. Goswami, T. R. Albright, A. Syed, A. S. Dutton, E. A. Smith, A. H. Winter, *J. Am. Chem. Soc.* **2018**, *140*, 7343–7346.
[14] H. Yu, J. Li, D. Wu, Z. Qiu, Y. Zhang, *Chem. Soc. Rev.* **2010**, *39*, 464–473.
[15] P. Wang, *Asian J. Org. Chem.* **2013**, *2*, 452–464.
[16] A. P. Gorka, R. R. Nani, M. J. Schnermann, *Acc. Chem. Res.* **2018**, *51*, 3226–3235.
[17] P. Hu, K. Berning, Y.-W. Lam, I. H.-M. Ng, C.-C. Yeung, M. H.-W. Lam, *J. Org. Chem.* **2018**, *83*, 12998–13010.
[18] X. Wang, J. A. Kalow, *Org. Lett.* **2018**, *20*, 1716–1719.
[19] A. Y. Vorobev, A. E. Moskalensky, *Comput. Struct. Biotechnol. J.* **2020**, *18*, 27–34.
[20] P. Štacko, P. Šebej, A. T. Veetil, P. Klán, *Org. Lett.* **2012**, *14*, 4918–4921.
[21] P. Vath, D. E. Falvey, L. A. Barnhurst, A. G. Kutateladze, *J. Org. Chem.* **2001**, *66*, 2887–2890.
[22] W. A. McHale, A. G. Kutateladze, *J. Org. Chem.* **1998**, *63*, 9924–9931.
[23] P. G. M. Wuts, *Greene's Protective Groups in Organic Synthesis*, John Wiley & Sons, Inc. **2014**.
[24] M. Yus, C. Nájera, F. Foubelo, *Tetrahedron* **2003**, *59*, 6147–6212.
[25] T. E. Burghardt, *J. Sulfur Chem.* **2005**, *26*, 411–427.
[26] D. K. Stevenson, L. K. Kwong, H. J. Vreman, *Clin. Chem.* **1984**, *30*, 1382–1386.
[27] H. J. Vreman, D. K. Stevenson, *Anal. Biochem.* **1988**, *168*, 31–38.
[28] M. Arık, K. Meral, Y. Onganer, *J. Lumin.* **2009**, *129*, 599–604.
[29] O. Valdes-Aguilera, D. C. Neckers, *Acc. Chem. Res.* **2002**, *22*, 171–177.
[30] G. R. Fleming, A. W. E. Knight, J. M. Morris, R. J. S. Morrison, G. W. Robinson, *J. Am. Chem. Soc.* **1977**, *99*, 4306–4311.
[31] P. Murasecco-Suardi, E. Gassmann, A. M. Braun, E. Oliveros, *Helv. Chim. Acta* **1987**, *70*, 1760–1773.
[32] L. Ludvíková, P. Friš, D. Heger, P. Šebej, J. Wirz, P. Klán, *Phys. Chem. Chem. Phys.* **2016**, *18*, 16266–16273.
[33] J. C. Scaiano, *J. Am. Chem. Soc.* **1980**, *102*, 7747–7753.
[34] C. S. Foote, *Science* **1968**, *162*, 963–970.
[35] C. S. Foote, *ACS Symp. Ser.* **1987**, *339*, 22–38.
[36] K. Gollnick, *Adv. Photochem., Vol. 6*, John Wiley & Sons **1968**, pp. 1–122.
[37] S. Kim, M. Fujitsuka, M. Miyata, T. Majima, *Phys. Chem. Chem. Phys.* **2016**, *18*, 2097–2103.
[38] R. P. Sabatini, M. F. Mark, D. J. Mark, M. W. Kryman, J. E. Hill, W. W. Brennessel, M. R. Detty, R. Eisenberg, D. W. McCamant, *Photochem. Photobiol. Sci.* **2016**, *15*, 1417–1432.
[39] V. E. Korobov, V. V. Shubin, A. K. Chibisov, *Chem. Phys. Lett.* **1977**, *45*, 498–501.
[40] M. N. Eberlin, *Eur. J. Mass Spectrom.* **2017**, *13*, 19–28.
[41] P. Chen, *Angew. Chem. Int. Ed.* **2003**, *42*, 2832–2847; *Angew. Chem.* **2003**, *115*, 2938–2954.
[42] L. Jašíková, M. Anania, S. Hybelbauerová, J. Roithová, *J. Am. Chem. Soc.* **2015**, *137*, 13647–13657.
[43] L. Sleno, D. A. Volmer, *J. Mass Spectrom.* **2004**, *39*, 1091–1112.
[44] L. Jašíková, J. Roithová, *Chem. Eur. J.* **2018**, *24*, 3374–3390.
[45] J. Roithová, *Chem. Soc. Rev.* **2012**, *41*, 547–559.
[46] L. MacAleese, P. Maître, *Mass Spectrom. Rev.* **2007**, *26*, 583–605.
[47] J. Roithová, A. Gray, E. Andris, J. Jašík, D. Gerlich, *Acc. Chem. Res.* **2016**, *49*, 223–230.
[48] J. Zelenka, J. Roithová, *ChemBioChem* **2020**, (in print).
[49] M. Montalti, A. Credi, L. Prodi, M. T. Gandolfi, *Handbook of Photochemistry*, 3rd ed., CRC Press Boca Raton **2006**.
[50] Y. Onganer, E. L. Quitevis, *J. Phys. Chem.* **1992**, *96*, 7996–8001.
[51] X.-F. Zhang, J. Zhang, X. Lu, *J. Fluoresc.* **2015**, *25*, 1151–1158.
[52] R. E. Barnett, W. P. Jencks, *J. Am. Chem. Soc.* **1967**, *89*, 5963–5964.
[53] R. E. Barnett, W. P. Jencks, *J. Am. Chem. Soc.* **1969**, *91*, 6758–6765.
[54] A. Specht, S. Loudwig, L. Peng, M. Goeldner, *Tetrahedron Lett.* **2002**, *43*, 8947–8950.
[55] W. Lin, D. S. Lawrence, *J. Org. Chem.* **2002**, *67*, 2723–2726.
[56] A. P. Kostikov, V. V. Popik, *Org. Lett.* **2008**, *10*, 5277–5280.
[57] M. El Baraka, M. Deumié, P. Viallet, T. J. Lampidis, *J. Photochem. Photobiol. A* **1991**, *56*, 295–311.
[58] E. Baciocchi, C. Crescenzi, O. Lanzalunga, *Tetrahedron* **1997**, *53*, 4469–4478.
[59] C. J. Regan, D. P. Walton, O. S. Shafaat, D. A. Dougherty, *J. Am. Chem. Soc.* **2017**, *139*, 4729–4736.
[60] M. Bettoni, T. Del Giacco, M. Stradiotto, F. Elisei, *J. Org. Chem.* **2015**, *80*, 8001–8008.
[61] M. Kamata, H. Otogawa, E. Hasegawa, *Tetrahedron Lett.* **1991**, *32*, 7421–7424.
[62] G. Oksdath-Mansilla, V. Hajj, D. M. Andrada, J. E. Argüello, J. Bonin, M. Robert, A. B. Peñéñory, *J. Org. Chem.* **2015**, *80*, 2733–2739.
[63] M. J. Frisch, G. W. Trucks, H. B. Schlegel, G. E. Scuseria, M. A. Robb, J. R. Cheeseman, G. Scalmani, V. Barone, B. Mennucci, G. A. Petersson, H. Nakatsuji, M. Caricato, X. Li, H. P. Hratchian, A. F. Izmaylov, J. Bloino, G. Zheng, J. L. Sonnenberg, M. Hada, M. Ehara, K. Toyota, R. Fukuda, J. Hasegawa, M. Ishida, T. Nakajima, Y. Honda, O. Kitao, H. Nakai, T. Vreven, J. A. Montgomery Jr., J. E. Peralta, F. Ogliaro, M. Bearpark, J. J. Heyd, E. Brothers, K. N. Kudin, V. N. Staroverov, R. Kobayashi, J. Normand, K. Raghavachari, A. Rendell, J. C. Burant, S. S. Iyengar, J. Tomasi, M. Cossi, N. Rega, J. M. Millam, M. Klene, J. E. Knox, J. B. Cross, V. Bakken, C. Adamo, J. Jaramillo, R. Gomperts, R. E. Stratmann, O. Yazyev, A. J. Austin, R. Cammi, C. Pomelli, J. W. Ochterski, R. L. Martin, K. Morokuma, V. G. Zakrzewski, G. A. Voth, P. Salvador, J. J. Dannenberg, S. Dapprich, A. D. Daniels, O. Farkas, J. B. Foresman, J. V. Ortiz, J. Cioslowski, D. J. Fox, *Gaussian 09, revision D.01*; Gaussian, Inc.: Wallingford, CT **2009**.
[64] Y. Zhao, D. G. Truhlar, *J. Chem. Phys.* **2006**, *125*, 194101.
[65] F. Weigend, R. Ahlrichs, *Phys. Chem. Chem. Phys.* **2005**, *7*, 3297.
[66] S. Grimme, J. Antony, S. Ehrlich, H. Krieg, *J. Chem. Phys.* **2010**, *132*, 154104.
[67] H. D. Dakin, *J. Am. Chem. Soc.* **1909**, *42*, 477–498.
[68] H. L. J. Bäckström, *J. Am. Chem. Soc.* **1927**, *49*, 1460–1472.
[69] M. Sankar, E. Nowicka, E. Carter, D. M. Murphy, D. W. Knight, D. Bethell, G. J. Hutchings, *Nat. Commun.* **2014**, *5*.
[70] J. R. McNesby, C. A. Heller, *Chem. Rev.* **1954**, *54*, 325–346.
[71] C. A. McDowell, L. K. Sharples, *Can. J. Chem.* **1958**, *36*, 251–257.
[72] M.-Y. Ngai, A. Banerjee, Z. Lei, *Synthesis* **2018**, *51*, 303–333.
[73] L. Vanoye, A. Favre-Réguillon, A. Aloui, R. Philippe, C. de Bellefon, *RSC Adv.* **2013**, *3*, 18931.
[74] M. Hajimohammadi, N. Safari, H. Mofakham, A. Shaabani, *Tetrahedron Lett.* **2010**, *51*, 4061–4065.
[75] L. A. P. Antony, T. Slanina, P. Šebej, T. Šolomek, P. Klán, *Org. Lett.* **2013**, *15*, 4552–4555.
[76] J. D. Crounse, H. C. Knap, K. B. Ørnsø, S. Jørgensen, F. Paulot, H. G. Kjaergaard, P. O. Wennberg, *J. Phys. Chem. A* **2012**, *116*, 5756–5762.
[77] H. G. Kjaergaard, H. C. Knap, K. B. Ørnsø, S. Jørgensen, J. D. Crounse, F. Paulot, P. O. Wennberg, *J. Phys. Chem. A* **2012**, *116*, 5763–5768.
[78] W.-U. Palm, *Photochem. Photobiol. Sci.* **2018**, *17*, 964–974.
[79] A. D. Britt, W. B. Moniz, *J. Org. Chem.* **1973**, *38*, 1057–1059.
[80] P. C. Beaumont, D. G. Johnson, B. J. Parsons, *J. Photochem. Photobiol. A* **1997**, *107*, 175–183.
[81] T. J. Chozinski, L. A. Gagnon, J. C. Vaughan, *FEBS Lett.* **2014**, *588*, 3603–3612.
[82] S. van de Linde, I. Krstić, T. Prisner, S. Doose, M. Heilemann, M. Sauer, *Photochem. Photobiol. Sci.* **2011**, *10*, 499–506.
[83] H. Görner, *Photochem. Photobiol. Sci.* **2008**, *7*, 371.
[84] C. Chatgilialoglu, D. Crich, M. Komatsu, I. Ryu, *Chem. Rev.* **1999**, *99*, 1991–2070.
[85] J. Zelenka, R. Cibulka, J. Roithová, *Angew. Chem. Int. Ed.* **2019**, *58*, 15412–15420.
[86] S. Chen, M. S. Hossain, F. W. Foss, *Org. Lett.* **2012**, *14*, 2806–2809.
[87] Y.-R. Luo, *Comprehensive Handbook of Chemical Bond Energies*, CRC Press, Boca Raton **2007**.
[88] J. R. R. Majjigapu, A. N. Kurchan, R. Kottani, T. P. Gustafson, A. G. Kutateladze, *J. Am. Chem. Soc.* **2005**, *127*, 12458–12459.
[89] Note that all IRPD spectra reported in this work contain more bands than those predicted by the theoretical calculations for individual ions. This is most likely associated with different conformations of piperidine groups with respect to the xanthene backbone and with respect to each other.
[90] E. Bodo, A. Ciavardini, A. Giardini, A. Paladini, S. Piccirillo, F. Rondino, D. Scuderi, *Chem. Phys.* **2012**, *398*, 124–128.

Manuscript received: May 12, 2020
Revised manuscript received: July 12, 2020